Analyses of shear-wall panels with a composite plasticity model

ANALYSES OF SHEAR-WALL PANELS WITH A COMPOSITE PLASTICITY MODEL

PETER H. FEENSTRA and RENE DE BORST*
Delft University of Technology
Department of Civil Engineering
P.O. Box 5048, 2600 GA Delft, The Netherlands.

and

JAN G. ROTS†
TNO Building and Construction Research
P.O. Box 49, 2600 AA Delft, The Netherlands.

Abstract. A constitutive model for concrete is presented which is formulated within the framework of incremental plasticity. The major improvement of the model is the stable and accurate algorithm which can be derived for tension, compression as well as tension-compression regimes. The analyses of shear-wall panels show that the composite plasticity model is well capable to describe the behavior of these type of structures.

Key words: finite element analysis, reinforced concrete

1. Introduction

A well established constitutive model for concrete cracking is the fixed multi-directional crack model which allows for a number of non-orthogonal cracks, [1] [2]. To analyze structures which are in a state of compression-tension, e.g. shear-wall panels, the crack model can be combined with a plasticity model to describe crack formation and crushing [1], but this combination has been reported to result in numerical difficulties, [3]. Because the major goal of this study is the development of stable numerical tools to analyze reinforced concrete structures, a different model has been formulated to solve both the problem of overestimation of the failure load with the fixed smeared crack model [2], and the numerical problems in the tension-compression region.

2. Constitutive model

In this study we assume that the constitutive behavior of concrete is governed by two yield functions, $f_1(\boldsymbol{\sigma}, \kappa_1)$ and $f_2(\boldsymbol{\sigma}, \kappa_2)$, where the internal variables, κ_1 and κ_2, represent the accumulated damage in the material due to cracking and crushing respectively. Comparison with the experimental data of [4] indicates that a composite yield contour can be defined such that a Rankine yield criterion is used to model the tension-tension region and a Von Mises yield function models the compressive stress states, see Figure 1. The formulation of

* Also at Eindhoven University of Technology
† Also at Delft University of Technology

G.M.A. Kusters and M.A.N. Hendriks (eds.), DIANA Computational Mechanics '94, 349-358.

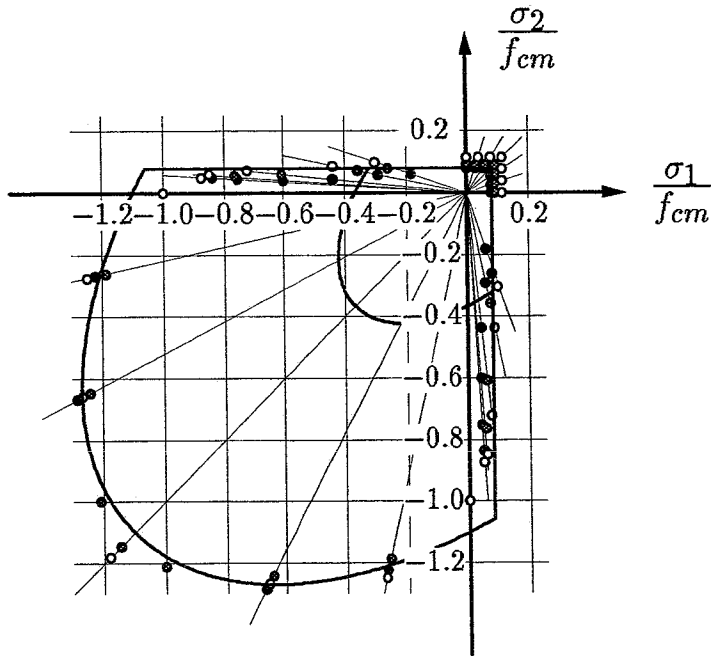

Fig. 1. Composite yield surface and experimental data

the composite yield criterion is then given by

$$f_1 = (\frac{1}{2}\boldsymbol{\sigma}^T\mathbf{P}_1\boldsymbol{\sigma})^{\frac{1}{2}} + \frac{1}{2}\boldsymbol{\pi}^T\boldsymbol{\sigma} - \bar{\sigma}_1(\kappa_1) \tag{1}$$

$$f_2 = (\frac{1}{2}\boldsymbol{\sigma}^T\mathbf{P}_2\boldsymbol{\sigma})^{\frac{1}{2}} - \bar{\sigma}_2(\kappa_2) \tag{2}$$

For the Rankine criterion the projection matrix $\mathbf{P}_1$ and the projection vector $\boldsymbol{\pi}$ are given by

$$\mathbf{P}_1 = \begin{bmatrix} \frac{1}{2} & -\frac{1}{2} & 0 & 0 \\ -\frac{1}{2} & \frac{1}{2} & 0 & 0 \\ 0 & 0 & 0 & 0 \\ 0 & 0 & 0 & 2 \end{bmatrix} \qquad \boldsymbol{\pi} = \{1,1,0,0\}^T \tag{3}$$

respectively. The Von Mises yield function is determined solely by the projection matrix $\mathbf{P}_2$ which is given by

$$\mathbf{P}_2 = \begin{bmatrix} 2 & -1 & -1 & 0 \\ -1 & 2 & -1 & 0 \\ -1 & -1 & 2 & 0 \\ 0 & 0 & 0 & 6 \end{bmatrix} \tag{4}$$

The $\bar{\sigma}_1 - \kappa_1$ relation for the Rankine yield criterion is assumed to be a linear relationship according to

$$\bar{\sigma}_1 = f_{ct,m}(1 - \frac{\kappa_1}{\kappa_{1,u}}) \tag{5}$$

in which the tensile strength $f_{ct,m}$ is determined from the compressive strength according to the CEB-FIP model code [6]. The ultimate damage parameter $\kappa_{1,u}$ is calculated by

$$\kappa_{1,u} = \frac{2G_f^{rc}}{h f_{ct,m}} \tag{6}$$

where h denotes the equivalent length. In a finite element calculation this equivalent length should correspond to a representative dimension of the mesh size, as pointed out by many authors, see e.g. [2] and [5]. In reinforced concrete usually a number of cracks develop during the process of loading until the cracking process stabilizes and no further cracks develop in the structure. The crack spacing at stabilized cracking is determined mainly by the amount of reinforcement. It is assumed in this study that the total amount of fracture energy in reinforced concrete, G_f^{rc}, can be determined by the tensile fracture energy of a single crack G_f and the average crack spacing l_s. Since the tensile fracture energy, G_f, is assumed to be a material parameter according to [6], only the average crack spacing has to be determined. The average crack spacing is a function of the bar diameter, the concrete cover and the reinforcement ratio according to [6], which reads

$$l_s = \frac{2}{3} \left(2\, s_0 \; + \; \frac{\phi_s}{\alpha \rho_{s,eff}} \right) \tag{7}$$

with the effective reinforcement ratio $\rho_{s,eff}$ determined by

$$\rho_{s,eff} \; = \; \frac{A_s}{A_{c,eff}} \tag{8}$$

The effective tension area, $A_{c,eff} = h_{eff} b$, is estimated according to the CEB-FIP recommendations with the relation

$$h_{eff} = min \left\{ 2.5 \left(c \; + \; \frac{\phi_{eq}}{2} \right) \; , \; \frac{t}{2} \right\} \tag{9}$$

with c the concrete cover on the reinforcement, ϕ_{eq} the equivalent bar diameter of the reinforcement and t the thickness of the structure. The effective tension area is calculated with the equivalent bar diameter of the reinforcing grid which is determined by

$$\phi_{eq} = \frac{\phi_p \, \rho_p + \phi_q \, \rho_q}{\rho_p + \rho_q} \tag{10}$$

with the reinforcement ratios ρ_p and ρ_q in the p- and q-directions of the reinforcing grid, respectively. The diameter of the reinforcement is given by ϕ_p and ϕ_q in the p- and q-direction respectively. The average crack spacing can now be calculated in the two directions of the reinforcing grid and when the cracks form at inclined angles with the reinforcing directions, the average crack spacing is calculated with the following expression [6]

$$l_s = \left(\frac{|\cos \alpha|}{l_{s,p}} + \frac{|\sin \alpha|}{l_{s,q}} \right)^{-1} \tag{11}$$

where α denotes the angle between the reinforcement in the p-direction and the direction of the principal tensile stress at incipient cracking. With this approach, the fracture energy in reinforced concrete can be assessed on the basis of the fracture energy of concrete, the reinforcement properties and the angle between reinforcement and the principal stress at incipient cracking. In this fashion, the tension-softening of reinforced concrete has been formulated in a rational manner.

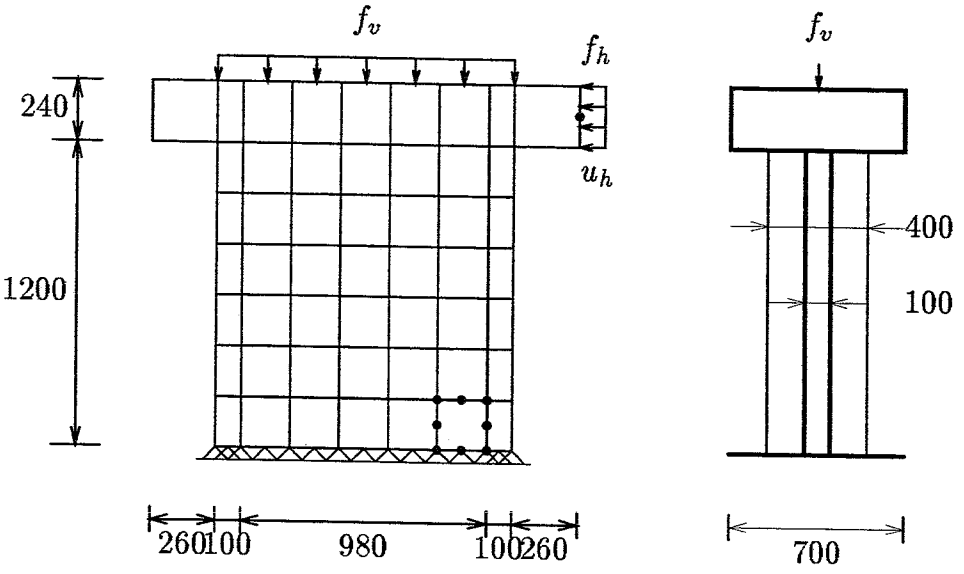

Fig. 2. Panels S1 and S2. Measures in [mm]

The $\bar{\sigma}_2 - \kappa_2$ relation for the Von Mises yield criterion is assumed to be given by a parabolic relationship which reads

$$\bar{\sigma}_2 = \begin{cases} \frac{1}{3} f_{cm}(1 + 4\frac{\kappa_2}{\kappa_e} - 2\frac{\kappa_2^2}{\kappa_e^2}) \;\; if \;\; \kappa_2 < \kappa_e \\ \\ f_{cm}(1 - \frac{(\kappa_2 - \kappa_e)^2}{(\kappa_{2,u} - \kappa_e)^2}) \;\; if \;\; \kappa_e \leq \kappa_2 < \kappa_{2,u} \end{cases} \tag{12}$$

with the mean compressive strength f_{cm}. The maximum compressive strength will be reached at an equivalent strain κ_e which is determined irrespective of element size or compressive fracture energy and reads

$$\kappa_e = \frac{4 f_{cm}}{3 E_c} \tag{13}$$

The maximum equivalent strain $\kappa_{2,u}$ is related to a compressive fracture energy G_c and to the element size through the equivalent length h and reads

$$\kappa_{2,u} = 1.5 \frac{G_c}{h f_{cm}} \tag{14}$$

Experimental data of the compressive fracture energy G_c have been provided by [7] where it has been found that G_c ranges from 50 to 100 times the tensile fracture energy. Analyses of deep beams with the composite plasticity model [8] showed that the compressive fracture energy G_c for normal strength concrete is about $50[Nmm/mm^2]$, which will be used in the analyses of the shear-wall panels.

3. Shear-wall panels

The analysis of shear-wall panels is a good example of the possible application of the developed model because the stress state in the panels can be considered to be in tension-compression. The panels which will be analyzed have been tested at the E.T.H. Zürich by [9]. The program consisted of a series of panels with flanges and without flanges, with different reinforcement lay-outs and initial vertical confinement stresses. The panels are

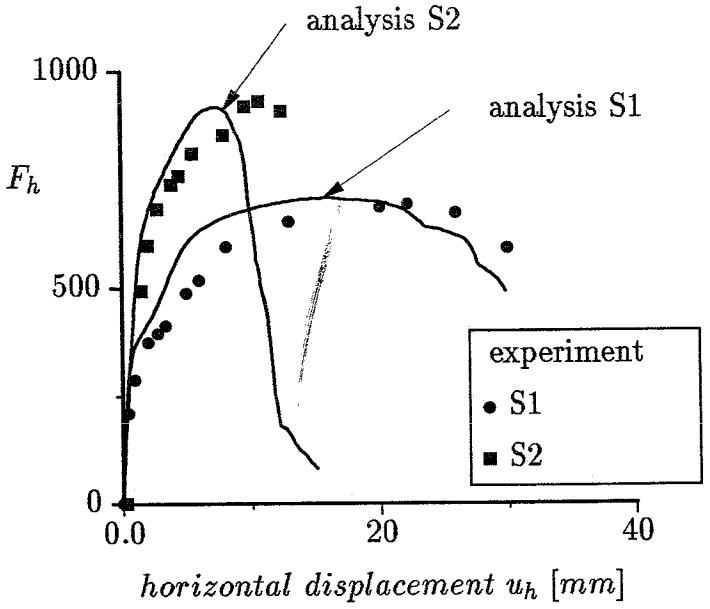

Fig. 3. Panels S1 and S2. Load - displacement diagram

supported on a base block and loaded through a thick top slab. The panels are initially loaded by a vertical compressive force and then by a horizontal force.

The material properties have been averaged from the experimental data in order to simulate the behavior of the panels in a qualitative manner. The compressive strength $f_{cm} = 27.5[N/mm^2]$ and the tensile strength $f_{ct,m} = 2.2[N/mm^2]$. The elastic properties have been assumed to be Young's modulus $E_c = 30000[N/mm^2]$ and Poisson's ratio $\nu = 0.15$. The tensile fracture energy is assessed according to [6] as $G_f = 0.07[Nmm/mm^2]$ and the compressive fracture energy is assumed $G_c = 50[Nmm/mm^2]$. The Young's modulus of the steel $E_s = 210000[N/mm^2]$ and the yield strength $f_{sy} = 574[N/mm^2]$ with linear hardening. An additional stiffness component has been modeled in the direction of the reinforcement to account for the bond between the cracks of the stabilized crack pattern. For details see [10].

The results of the analysis will be presented by plotting the active cracks, the integration points which are in a compressive plastic state and the principal stresses. The active cracks are defined as those cracks for which the internal parameter κ_1 is equal or greater than $0.5\kappa_{1,u}$.

4. Shear-wall panels with flanges

Two identical panels with flanges have been analyzed, i.e. panels S1 and S2. The main objective of these two experiments is to study the influence of the initial vertical compressive load. The initial vertical load of panel S1 results in a vertical stress of $2.5[N/mm^2]$ while the initial vertical stress of panel S2 is equal to $10.0[N/mm^2]$.

The finite element discretization is depicted in Figure 2 with quadratic plane-stress elements with a nine-point Gaussian integration for both the reinforcement and the matrix material. The reinforcement is applied by two reinforcing grids in two directions with reinforcement ratios $\rho_x = 0.0103$ and $\rho_y = 0.0116$. The grids have rebars with a diameter of $8[mm]$ and a clear cover of $10[mm]$. The top slab has been modeled with linear-elastic elements without reinforcement, whereas the supporting block has been replaced by fixed supports in the x- and y-direction. The horizontal displacement u_h of the top slab has been

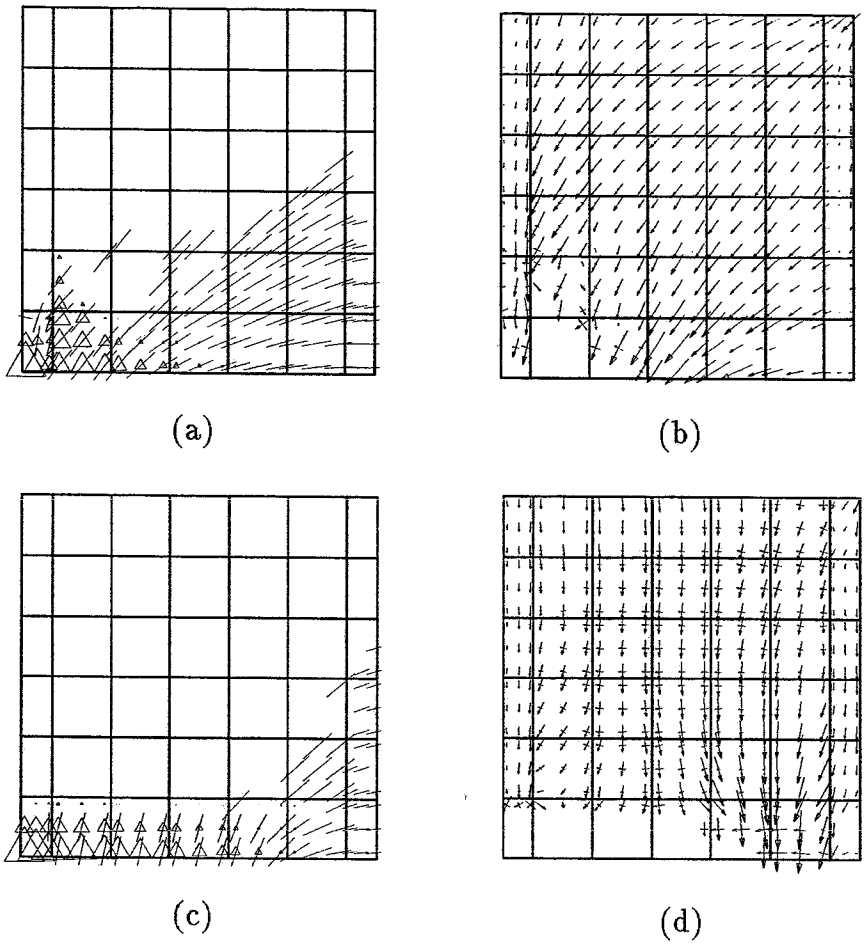

Fig. 4. Results of panels S1 and S2 at ultimate displacement. Active cracks and plastic points: (a) S1; (c) S2. Principal stresses: (b) S1; (d) S2

monitored and compared with the experimental load-displacement curves.

The load-displacement diagrams of the panels are shown in Figure 3, which shows a reasonable agreement between the experimental and the calculated responses for both panels. The results for panel S1 at the ultimate displacement of $30[mm]$ are shown in Figure 4(a) and 4(b). The panel is heavily cracked with plastic points in the bottom-left corner of the panel. The results show the failure mechanism which is governed by compressive softening of the concrete. In the ultimate state, the concrete in the bottom-left corner transfers no stress anymore, which is in agreement with the experimentally observed failure mechanism where the concrete was crushed in the bottom-left corner of the panel and in the flange at the compression side.

The larger initial vertical stress of panel S2 increases the ultimate load of the structure but decreases the ductility of the panel dramatically, see Figure 3. The agreement between the ultimate load of the experiment and the calculated maximum load is good. The experimental failure mechanism was rather explosive and caused a complete loss of load-carrying capacity which can be explained by the brittle behavior of the panel after maximum load. The results for the ultimate displacement u_h of $15[mm]$ are shown in Figure 4(c) and 4(d) in which the redistribution of internal forces in the panel can clearly be observed. The complete loss of stiffness in the bottom of the panel can be observed from Figure 4(d) where the principal stresses are depicted.

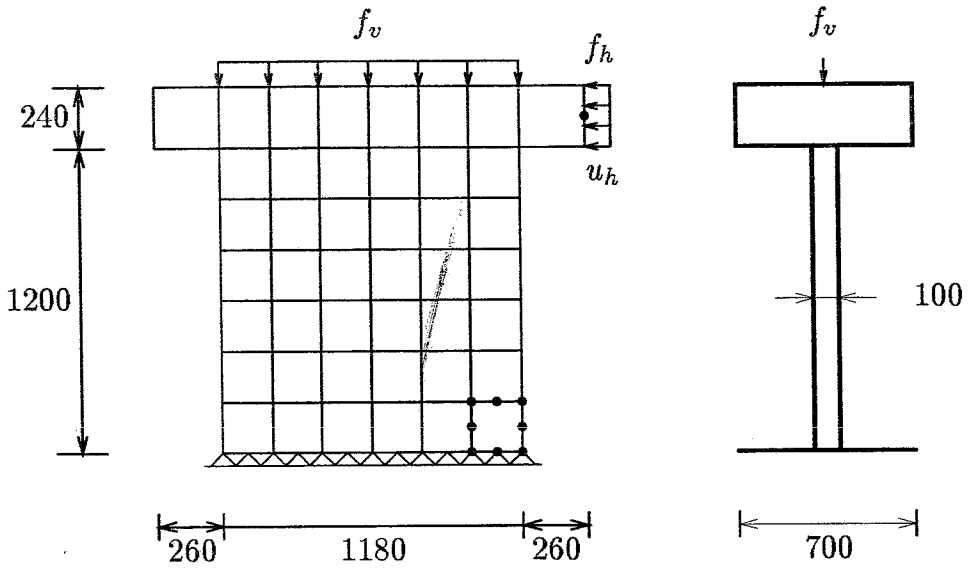

Fig. 5. Panels S4, S9 and S10. Measures in [mm]

5. Shear-wall panels without flanges

Next, three panels without flanges will be presented, panels S4, S10 and S9. The finite element discretization is depicted in Figure 5 with quadratic plane-stress elements with a nine-point Gaussian integration for both the reinforcement and the element. The reinforcement is applied by two reinforcing grids in two directions. The grids have rebars with a diameter of 8$[mm]$ and a clear cover of 10$[mm]$. The top slab has been modeled with linear-elastic elements without reinforcement, whereas the supporting block has been replaced by fixed supports in the x- and y-direction.

The initial vertical load of panel S4 results in a vertical stress that is approximately equal to that in panel S1. The panel is reinforced with two orthogonal grids with a reinforcement ratio $\rho_x = 0.0103$ and $\rho_y = 0.0105$. The load-displacement diagram, shown in Figure 6, shows a reasonable agreement with the experimental observed behavior. The panel behaves in a rather ductile manner which has also been observed for panel S1. The results at the final displacement of 20 $[mm]$ are shown in Figure 7(a) and 7(b) where the active cracks and plastic points, and the principal stresses are shown, respectively. It is obvious from these results that the failure mode is related to concrete crushing in the bottom-left corner of the panel.

Panel S10 is a panel with a reinforcement ratio $\rho_x = 0.0098$ and $\rho_y = 0.0100$ with additional reinforcement in the tension side of the panel, which can be considered as a panel with a *hidden tensile flange*. This results in an increase of the ultimate load, but a decrease in the ductility, see Figure 6. The results at the final displacement of 20 $[mm]$ are shown in Figure 7(c) and 7(d), where a remarkable resemblance can be observed with the failure pattern of panel S2, see Figure 4(c) and 4(d).

The last analysis is the simulation of panel S9 which can be considered as a major challenge since this panel is only reinforced in the vertical direction. This will result in an unstable behavior during the formation of the cracks until a stable crack pattern has been obtained. The finite element discretization is depicted in Figure 5 and is equal to the panels S4 and S10. The reinforcement in this panel is applied by two unidirectional reinforcing grids with a reinforcement ratio $\rho_x = 0.0001$[1] and $\rho_y = 0.00525$. The grids have again

[1] assures non-zero stiffness in the x-direction for fully cracked elements

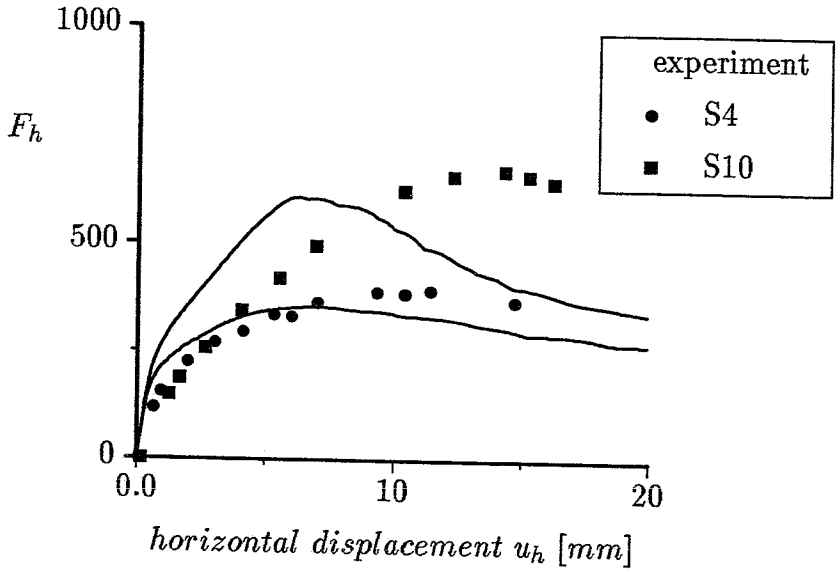

Fig. 6. Panels S4 and S10. Load - displacement diagram

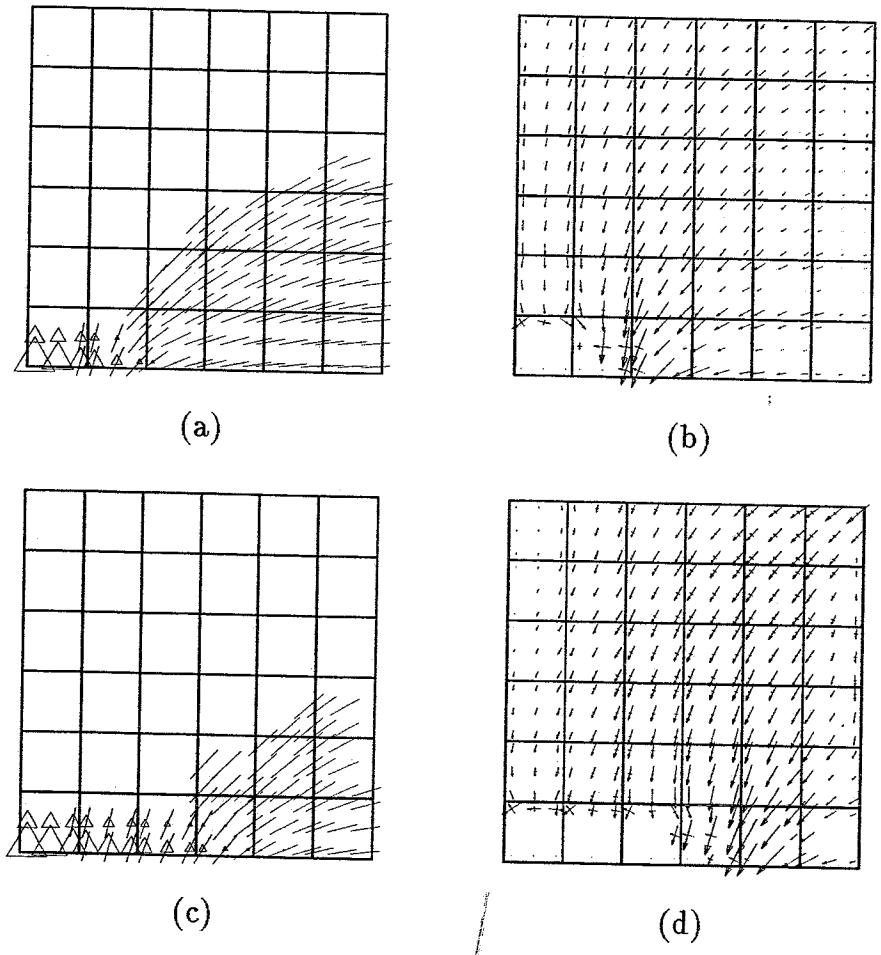

Fig. 7. Results of panels S4 and S10 at ultimate displacement. Active cracks and plastic points: (a) S4; (c) S10. Principal stresses: (b) S4; (d) S10

rebars with a diameter of 8 [mm] and a clear cover of 10 [mm]. In comparison with the other panels, the reinforcement ratio of this panel is small which increases the numerical difficulties.

The load-displacement diagram is shown in Figure 8, which shows the typical behavior of these type of panels. In the initial part of the load-displacement diagram the cracks

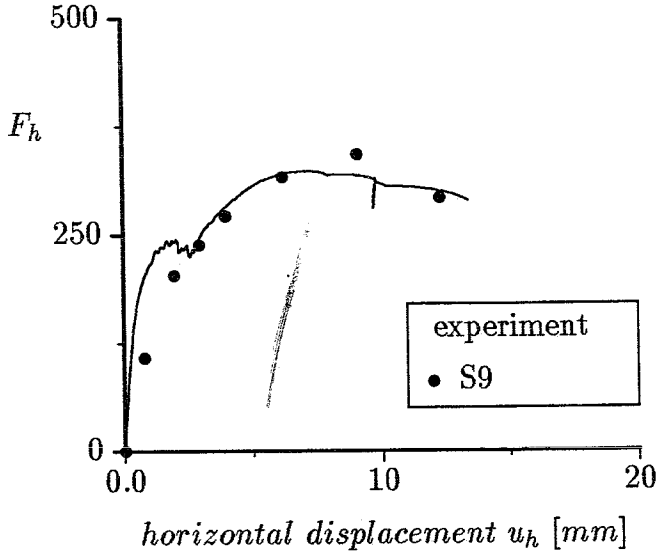

Fig. 8. Panel S9. Load - displacement diagram

are initiated and the process of crack growth results in a globally horizontal plateau but many local limit points can be observed. During this phase, small load increments had to be taken in order to obtain a non-diverging solution. In this stage of the calculation different non-converging steps have been obtained. During these non-converging steps a multiple equilibrium state has been triggered which is inherent to these type of structures. Even in a later stage, non-converging steps have been encountered which resulted in one case in a spurious unloading/reloading, see Figure 8 at a displacement of approximately 10 [mm]. The agreement with the experiment is quite poor in the initial, uncracked, part of the load-displacement diagram which might be caused by an overestimation of the Young's modulus. The failure load is nevertheless in reasonable accordance with the experimental failure load and the post-peak behavior shows also the rather ductile behavior of the panel.

The results for panel S9 at the ultimate displacement of 13 [mm] are shown in Figure 9(a) and 9(b). The panel is heavily cracked in almost the entire panel with a small area with plastic points in the bottom-left corner of the panel. The load-carrying capacity through a compressive strut can clearly be observed from the principal stresses in Figure 9(b). The part of the panel which is in a compressive failure state is small in comparison with the other panels, which can be explained by the relatively small reinforcement ratio. The reinforcement yields at the maximum load which results in the ductile post-peak behavior.

6. Concluding remarks

It has been shown with the analyses of the shear-wall panels that the developed composite yield model is capable to simulate the experimental load-displacement diagram. The failure mechanism which has been found is in reasonable agreement with the experimental failure mechanism. Further research is necessary to develop the concept of compressive fracture energy.

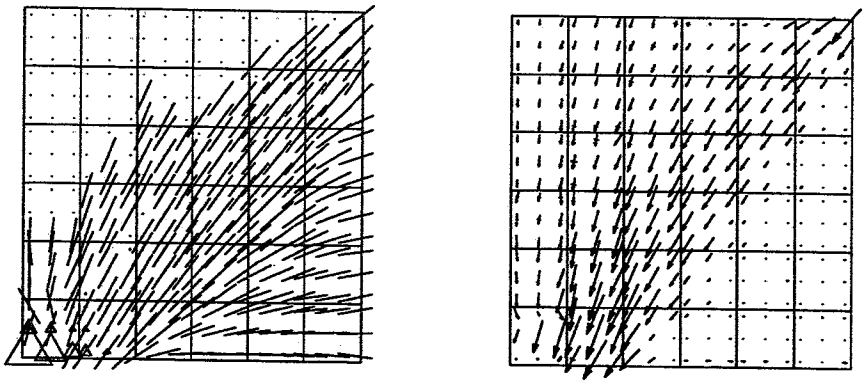

Fig. 9. Results of panel S9 at ultimate displacement. (a) Active cracks and plastic points; (b) Principal stresses

Acknowledgements

The calculations have been carried out with a pilot-version of the *DIANA* finite element code. The financial support by the Netherlands Technology Foundation (STW) under grant DCT-72.1405 and by the Commission of the European Communities through the Brite-Euram project BE-3275 is gratefully acknowledged.

This publication has been written during a stay of the first author at the University of Colorado at Boulder, supported by a NATO-Science Fellowship.

References

1. De Borst, R. and Nauta, P.: 1985, 'Non-orthogonal cracks in a smeared finite element model', *Engrg. Comput.* Vol. no. **2**, pp. 35–46
2. Rots, J.G.: 1988, 'Computational modeling of concrete fracture', Dissertation, Delft University of Technology, The Netherlands.
3. Wang, Q.B., Van Der Vorm, P.L.J. and Blaauwendraad, J.: 1990, 'Failure of reinforced concrete panels. How accurate the models must be ?', in: *Computer Aided Analysis and Design of Concrete Structures*, eds. N. Bićanić *et al.*, Pineridge Press, pp. 153–163.
4. Kupfer, H.B. and Gerstle, K.H.: 1973, 'Behavior of concrete under biaxial stresses', *J. Engrg. Mech.* Vol. no. **99(4)**, 853–866.
5. Bažant, Z.P. and Oh, B.H.: 1983, 'Crack band theory for fracture of concrete', *Materials and Structures* RILEM, Vol. no. **93(16)**, pp. 155-177.
6. CEB-FIP: 1990, 'Model code 1990', Bulletin d'information, CEB.
7. Vonk, R.A.: 1992, 'Softening of concrete loaded in compression', Dissertation, Eindhoven University of Technology, The Netherlands.
8. Feenstra, P.H., De Borst, R. and Rots, J.G.: 1994, 'An energy-based composite plasticity model for concrete', in: *Computational modelling of concrete structures*, eds. H. Mang *et al.*, Pineridge Press, pp. 83–92.
9. Maier, J. and Thürlimann, B.: 1985, 'Bruchversuche an Stahlbetonscheiben', Report 8003-1, Eidgenössische Technische Hochschule Zürich, Switzerland.
10. Feenstra, P.H.: 1993, 'Computational aspects of biaxial stress in plain and reinforced concrete', Dissertation, Delft University of Technology, The Netherlands.